


 Cite this: *RSC Adv.*, 2021, 11, 19012

Acidity effects of medium fluids on anhydrous proton conductivity of acid-swollen block polymer electrolyte membranes†

 Takato Kajita, ^a Atsushi Noro, ^{*ab} Takahiro Seki, ^a Yushu Matsushita ^{‡a} and Naoki Nakamura ^c

Proton-conductive polymer electrolyte membranes (PEMs) were prepared by infiltrating sulfuric acid (Sa) or phosphoric acid (Pa) into a polystyrene-*b*-poly(4-vinylpyridine)-*b*-polystyrene (S-P-S) triblock copolymer. When the molar ratio of acid to pyridyl groups in S-P-S, *i.e.*, the acid doping level (ADL), is below unity, the P-block/acid phase in the PEMs exhibited a moderately high glass transition temperature (T_g) of ~ 140 °C because of consumption of acids for forming the acid-base complexes between the pyridyl groups and the acids, also resulting in almost no free protons in the PEMs; therefore, the PEMs were totally glassy and exhibited almost no anhydrous conductivity. In contrast, when ADL is larger than unity, the T_g s of the phase composed of acid and P blocks were lower than room temperature, due to the excessive molar amount of acid serving as a plasticizer. Such swollen PEMs with excessive amounts of acid releasing free protons were soft and exhibited high conductivities even without humidification. In particular, an S-P-S/Sa membrane with ADL of 4.6 exhibited a very high anhydrous conductivity of 1.4×10^{-1} S cm⁻¹ at 95 °C, which is comparable to that of humidified Nafion membranes. Furthermore, S-P-S/Sa membranes with lower T_g s exhibited higher conductivities than S-P-S/Pa membranes, whereas the temperature dependence of the conductivities for S-P-S/Pa is stronger than that for S-P-S/Sa, suggesting Pa with a lower acidity would not be effectively dissociated into a dihydrogen phosphate anion and a free proton in the PEMs at lower temperatures.

Received 14th February 2021

Accepted 19th May 2021

DOI: 10.1039/d1ra01211h

rsc.li/rsc-advances

1. Introduction

Fuel cells can generate electrical energy together with water through an electrochemical reaction between hydrogen and oxygen gases; thus, they are highly promising as a clean power generation system.¹⁻³ In particular, polymer electrolyte fuel cells (PEFCs) with proton-conductive polymer electrolyte membranes (PEMs) have already been used in commercially available fuel cell vehicles (FCVs) and household fuel cell cogeneration systems.⁴⁻⁸ Perfluorosulfonic acid polymers such as Nafion® are the best-known proton-conductive PEMs.⁹⁻¹² Nafion membranes exhibit a very high proton conductivity of 0.1 S cm⁻¹ or higher

under humidification in the presence of water molecules at 70–90 °C,¹³⁻¹⁵ where the hydrophobic phase with fluorine moiety and the sulfonic acid group/water mixed phase are separated from each other at a microscopic scale.¹⁶⁻¹⁸ The former plays a part in keeping the membrane shape, and the latter serves as the proton-conductive paths. Hydrocarbon-based proton-conductive PEMs,^{19,20} such as sulfonated polyetheretherketone (PEEK),²¹⁻²³ polysulfone,²⁴⁻²⁸ polyphenylene,²⁹⁻³¹ and poly(styrene sulfonic acid),^{32,33} have also been widely studied; however, these PEMs exhibit almost no proton conductivity under dry conditions so that fuel cell reactions never occur. Thus, PEFCs using these PEMs require humidifiers or humidification systems to circulate water vapor, which complicates and upsizes the PEFC systems.

To simplify the PEFC systems, PEMs exhibiting moderate proton conductivities even without humidification have been actively studied.³⁴⁻⁴³ A representative example is a phosphoric acid (Pa)-doped polybenzimidazole (PBI) membrane that exhibits the low or moderate conductivities of 0.0056 S cm⁻¹ at 130 °C and 0.04 S cm⁻¹ at 190 °C.⁴⁴ Because of the lower conductivities, the PEM of Pa-doped PBI cannot be an alternative to the humidified Nafion membrane. Efforts have also been made to enhance the anhydrous proton conductivity of PEMs composed of acid-doped PBI. For example, a membrane

^aDepartment of Molecular & Macromolecular Chemistry, Graduate School of Engineering, Nagoya University, Furo-cho, Chikusa-ku, Nagoya 464-8603, Japan. E-mail: noro@nagoya-u.jp

^bInstitute of Materials Innovation, Institutes of Innovation for Future Society, Nagoya University, Furo-cho, Chikusa-ku, Nagoya 464-8601, Japan

^cFC Material Development Dept., Electrification & Environment Material Engineering Div., Advanced R&D and Engineering Company, Higashifuji Technical Center, TOYOTA Motor Corporation, 1200 Mishuku, Susono, Shizuoka, Japan

† Electronic supplementary information (ESI) available. See DOI: 10.1039/d1ra01211h

‡ Present address: Toyota Physical and Chemical Research Institute, 41-1, Yokomichi, Nagakute, Aichi 480-1192, Japan.



exhibiting the anhydrous conductivity of 0.038 S cm^{-1} at 140°C was prepared by hybridizing PBI and sulfonic-acid-modified silica and further doping Pa into the composite membrane.^{45–51} However, the conductivity was still lower than that of humidified Nafion membranes, probably because the ability to retain Pa in the membrane was not high; substantially, merely the surface of the PBI membranes might be dissolved in Pa due to the rigidity of PBI. To overcome the above mentioned problems, some Pa-doped composite membranes composed of sulfonated PEEK^{52–54} or ether bonds-incorporated PBI^{55–57} have also been developed, which exhibit high anhydrous conductivities due to the higher Pa doping level.

Another effective solution to the problem may be to prepare a vinyl-polymer-based PEM by infiltrating a nearly nonvolatile low-molecular-weight liquid serving as a proton carrier. Vinyl polymers have a primary structure composed of a relatively flexible C–C single bond instead of a rigid PBI with aromatic groups in the backbone chain, although a mixture with a large amount of low-molecular-weight liquid is typically a solution and cannot be used as a membrane at the operating temperature of the fuel cell. To make the mixture solid-like material, the polymer in the mixture should be chemically or physically cross-linked, and it can be swollen with the low-molecular-weight liquid of medium fluid serving as a proton carrier. Especially, a self-assembled block polymer^{58,59} that forms vitrified microdomains serving as physical cross-links^{60–62} is an excellent candidate material for anhydrous proton-conductive PEMs because of their thermoplastic property. There have been several studies of the preparation of anhydrous proton-conductive PEMs by infiltrating nearly nonvolatile ionic liquids⁶³ into block polymers. For example, Park and coworkers pioneeringly prepared a proton-conductive PEM exhibiting an anhydrous conductivity of 0.045 S cm^{-1} at 160°C by infiltrating an aprotic ionic liquid into a vinyl-based diblock copolymer with sulfonic acid groups.⁶⁴ Segalman and coworkers also prepared a PEM exhibiting an anhydrous conductivity of 0.01 S cm^{-1} at 140°C by incorporating a protic ionic liquid into a vinyl-based diblock copolymer,⁶⁵ whereas Lodge, Hillmyer, and coworkers reported a PEM exhibiting an anhydrous conductivity of 0.014 S cm^{-1} at 180°C by infiltrating a protic ionic liquid into a cross-linked diblock copolymer.⁶⁶ Despite this progress, the anhydrous conductivities of these proton-conductive PEMs are not still sufficiently higher than the hydrous conductivity of the conventional Nafion membrane.

Recently, we developed an anhydrous PEM exhibiting comparatively high conductivity over 0.1 S cm^{-1} at around 100°C , regardless of an anhydrous condition, by infiltrating a large amount of nearly nonvolatile sulfuric acid (Sa) into a chemically cross-linked vinyl-based poly(4-vinylpyridine) membrane *via* acid–base complexation and ionic interactions.⁶⁷ Furthermore, we prepared an anhydrous highly proton-conductive PEM by swelling a self-assembled polystyrene-*b*-poly(4-vinylpyridine)-*b*-polystyrene (S–P–S) triblock copolymer with Sa. In terms of tensile properties and processability, the block polymer-based PEM is superior to the chemically cross-linked PEM, indicating that the S–P–S membrane swollen with Sa is a promising anhydrous proton-conductive PEM.

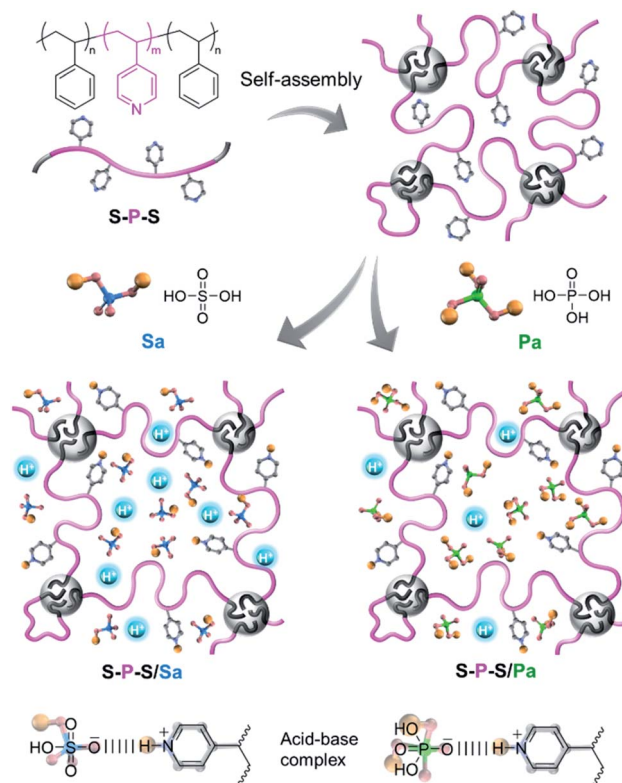


Fig. 1 Schematic illustration of the preparation of self-assembled block polymer-based proton-conductive PEMs.

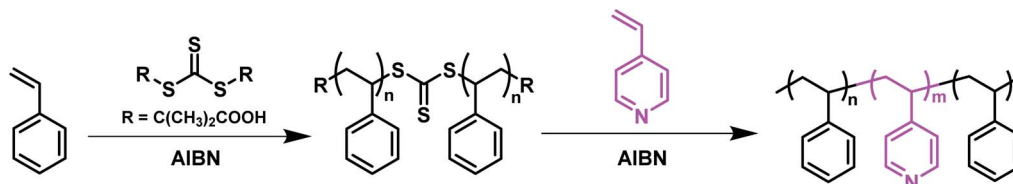
Nevertheless, the triblock copolymer-based PEM swollen with acid has been little investigated. Even the effects of different acids on the anhydrous proton conductivities of the PEMs have not been reported to date; however, anhydrous proton conductivities of the acid-swollen PEMs must be affected by the acidity of acidic liquids in the PEMs. Thus, investigation on acidity effects of the block polymer-based PEMs swollen with different acids is crucial to design highly proton-conductive PEMs under anhydrous conditions for next-generation fuel cells. In this study, by swelling the S–P–S block copolymer membrane with Sa or Pa, as shown in Fig. 1, we investigated the effects of different acidic liquids on the anhydrous proton conductivity of the triblock copolymer-based PEMs.

2. Experimental

2.1 Synthesis and characterization of a triblock copolymer

As shown in Scheme 1, S–P–S was synthesized by reversible addition–fragmentation chain transfer (RAFT) polymerization^{68,69} (see also Scheme S1, where the exact chemical structure of S–P–S with the RAFT agent residue is shown, ESI†). First, a styrene monomer (TCI Co., Ltd.) purified by passing through an alumina column (activated, basic, Brockmann I, Sigma-Aldrich) was polymerized by mixing a bifunctional RAFT agent of *S,S'*-bis(α,α' -dimethyl- α'' -acetic acid)trithiocarbonate⁷⁰ and a radical initiator of azobisisobutyronitrile (AIBN, Kishida Chemical Co., Ltd.), and the mixture was heated at 130°C for six





Scheme 1 Synthesis of S-P-S (note that the trithiocarbonate unit in the final product was omitted in the chemical structure for simplification).

hours, where the relatively high reaction temperature of 130 °C was adopted to promote the propagation reaction of styrene polymerization. After the polymerization, polystyrene (S) with a trithiocarbonate unit at the center of the polymer chain, *i.e.*, a macro-RAFT agent, was purified by reprecipitation. S-P-S was synthesized by mixing the macro-RAFT agent, AIBN, and a 4-vinylpyridine monomer (Sigma-Aldrich) and the mixture was heated at 80 °C for 1.5 hours, where the 4-vinylpyridine monomers were inserted next to the sulfur atoms of trithiocarbonate unit in the precursor S.^{68,69} See also details of synthesis of a similar block copolymer by RAFT polymerizations in the previous literature.^{67,71-73}

¹H NMR spectroscopy by an Ascend 500 MHz (Bruker Corp.) was used to determine the degree of polymerization of the precursor S, and composition of the block polymer. Deuterated chloroform was used as a solvent. Size exclusion chromatography (SEC) was also performed to determine the molecular weight distribution (\bar{M}) of polymers and to confirm successful synthesis of a block polymer. SEC was conducted using an HPLC system (HPLC Pump: Shimadzu LC-20AD; column oven: Shimadzu CTO-20A; RI detector: Shimadzu RID-10A) equipped with two TSKgel G5000H_{HR} columns (Tosoh Corp.) and *N,N*-dimethylformamide as the eluent solvent at 40 °C.

2.2 Preparation of acid-swollen membranes

Acid-swollen membranes with a thickness of ~0.5 mm were prepared by swelling neat S-P-S membranes with Sa or Pa, which are referred to as S-P-S/Sa or S-P-S/Pa, respectively. First, a solution of ~10 wt% was prepared by dissolving an S-P-S powder in pyridine, and then solution casting was conducted at 50 °C for two days followed by vacuum drying at 50 °C for one day. This resulted in the preparation of a neat S-P-S membrane. A 98 wt% aqueous solution of Sa or an 85 wt% aqueous solution of Pa was dissolved in methanol that more easily evaporates than water, and the S-P-S membrane was then immersed in the solutions, where a 20-fold weight of methanol to the neat S-P-S was used. After evaporating the volatile methanol and water from the solution at 50 °C for 12 hours, methanol was added again to homogeneously infiltrate the acid, followed by solution casting at 50 °C for 36 hours and vacuum drying at 50 °C for 24 hours. The weight content of acid in S-P-S-based PEMs was varied from 0 wt% to 80 wt%. Both S-P-S/Sa and S-P-S/Pa with lower than the acid content of 50 wt% were glassy and hard; in contrast, samples with an acid content of more than 60 wt% were soft and gel-like membranes (see also Fig. S1, ESI†). Note that polystyrene (S) cannot be dissolved in Sa and Pa, whereas poly(4-vinylpyridine) (P) is soluble in Sa and Pa (Fig. S2, ESI†);

therefore, Sa and Pa selectively infiltrated into the P phase of S-P-S membranes, where the vitrified S phase retained the shape. In other words, the membranes swollen with acid kept adopting the same morphology as the neat S-P-S membrane before swelling.⁷⁴⁻⁷⁶

The prepared membranes are coded as S-P-S/X(Y), where X represents the infiltrated acid, Sa or Pa, and Y denotes the weight percentage of acid in the membrane. The molar ratio of acid to pyridyl group in S-P-S is defined as the acid doping level (ADL),^{44,51} which is estimated from eqn (1).

$$\text{ADL} = \frac{n_{\text{acid}}}{n_{\text{base}}} = \frac{w_{\text{acid}}/M_{\text{acid}}}{w_{\text{base}}/M_{\text{base}}} = \frac{w_{\text{acid}}/M_{\text{acid}}}{w_{\text{S-P-S}}w'_{\text{P}}/M_{\text{P monomer}}} \quad (1)$$

where n_{acid} , w_{acid} , and M_{acid} are the molar amount, weight fraction, and molecular weight of acid, respectively, while n_{base} , w_{base} , and M_{base} are those of the base monomer unit, respectively. $w_{\text{S-P-S}}$, w'_{P} , and $M_{\text{P monomer}}$ are the weight fraction of S-P-S in the swollen membranes, weight fraction of P in neat S-P-S, and molecular weight of 4-vinylpyridine monomer (105 g mol⁻¹), respectively.

2.3 Measurements

Transmission electron microscopy (TEM) was used to observe the nanostructure of the neat S-P-S membrane, where the morphology depends on the volume fraction⁷⁷ of the S block in the S-P-S, the molecular weight⁷⁸ and \bar{D} ⁷⁹ of the S-P-S, and so on. The sample specimen of neat S-P-S membrane was embedded into epoxy resin, and the ultrathin section with a thickness of ~80 nm was prepared by a microtome in a wet condition, followed by staining with iodine (I₂) vapor at 60 °C for 40 minutes. The TEM observation was conducted with JEM-1400 (JEOL Ltd.) at an acceleration voltage of 120 kV.

To determine the conductivities of the PEMs, alternating current (AC) impedance spectroscopy was carried out with a potentio/galvanostat SP-300 (BioLogic Sciences Instruments) in the frequency range of 1 × 10⁰ to 1 × 10⁶ Hz at a signal amplitude of 50 mV by using a two-probe method that is easier to measure the impedance than a four-probe method. A test cell was prepared by fixing the distance between the platinum electrodes (l) at 7 mm and using the test specimen with sectional area (A) of ~2 mm².^{80,81} The temperature was controlled in the benchtop-type temperature and humidity chamber SH-242 (ESPEC Corp.) within a temperature range of 20–95 °C below the T_g of polystyrene (~100 °C) at no humidification, where the humidity in the chamber at all temperatures was close to 0 %RH which was determined with the thermohygrometer Testo-645 (Testo SE & Co. KGaA). Note that the



trithiocarbonate of the RAFT agent residue in the S-P-S would not be degraded within the temperature range adopted in this study.⁸² To estimate the conductivity, σ_{DC} , by using eqn (2), a bulk resistance (R) was evaluated from the Nyquist plot of the test specimen, by reading the extrapolated value of the plot on the horizontal axis, Z' , which is the real part of the complex impedance, $Z = Z' - iz''$, i.e., nonzero Z' intercept.^{83,84}

$$\sigma_{DC} = \frac{l}{AR} \quad (2)$$

The glass transition temperatures, T_{gS} , of the membranes were evaluated by differential scanning calorimetry (DSC) measurements using Q2000 (TA Instruments Inc.) with a heating rate of $10\text{ }^{\circ}\text{C min}^{-1}$ in the temperature range of $-90\text{ }^{\circ}\text{C}$ to $180\text{ }^{\circ}\text{C}$.

3. Results and discussion

3.1 Synthesis and characterizations of a block polymer

S-P-S was synthesized through two-step RAFT polymerization. Fig. 2a shows a ^1H NMR spectrum of S-P-S, and Fig. 2b shows SEC chromatograms of S-P-S and the precursor S. The number-average molecular weight of S ($M_{n,S}$) was determined to be 31k according to end-group analysis using the ^1H NMR spectrum (see also Fig. S3, ESI[†]). SEC measurements revealed that D s of S and S-P-S were 1.1 and 1.8, respectively, where the relatively

large D of S-P-S was probably caused by synthesizing relatively high molecular weight polymers. From the peak shift to a lower elution time compared to the peak of S, successful synthesis of S-P-S was confirmed. The mole fraction of the S block in S-P-S was determined to be 0.067 with ^1H NMR spectroscopy by comparing the integral of peaks from 8.0 to 8.6 ppm originating from two protons (H^e) on the pyridyl groups of the P block with that of peaks from 6.0 to 7.2 ppm originating from five protons (H^a , H^b and H^c) on the phenyl groups of the S block and two protons (H^d) on the pyridyl groups of the P block (Fig. 2a). By using the mole fraction of S in the block polymer and the $M_{n,S}$ estimated by the end-group analysis, w'_P and the total number-average molecular weight of S-P-S were estimated to be 0.93 and 461k, respectively. The volume fraction of the S block in S-P-S (ϕ_S) was 0.074, which was calculated from the bulk densities of S (1.05 g cm^{-3}) and P (1.17 g cm^{-3}).

A TEM image of a neat S-P-S membrane is shown in Fig. 2c, where the S phase appears brighter while the P phase does darker because of I_2 vapor staining. A brighter spherical S phase was observed in the darker P phase as a matrix. The distance between the domains (D) was estimated to be $\sim 40\text{ nm}$ in the TEM image, which roughly agreed with where spherical domains are assumed to be packed in a body-centered cubic (bcc) manner and q^* (0.13 nm^{-1}) is a scattering vector of the SAXS profile as shown in Fig. S4 (ESI[†]). Since Sa and Pa selectively infiltrated into the P phase of S-P-S membranes (see Fig. S2, ESI[†]), the membranes swollen with acid probably keep adopting the spherical morphology as the neat S-P-S membrane before swelling.^{74–76}

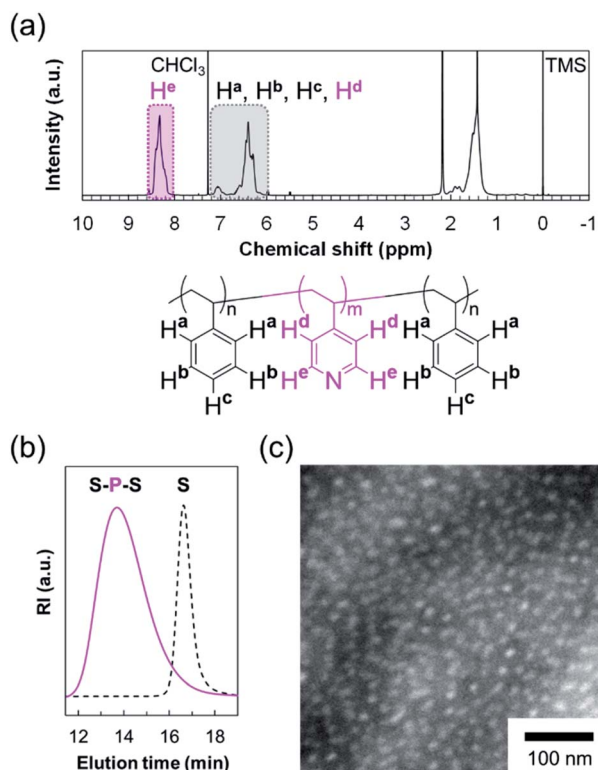


Fig. 2 (a) ^1H NMR spectrum and the chemical structure of S-P-S synthesized. (b) SEC chromatograms of S-P-S (solid line) and precursor S (dashed line). (c) A TEM image of the neat S-P-S membrane.

3.2 Anhydrous conductivity of acid-swollen S-P-S membranes

AC impedance spectroscopy was performed to determine anhydrous conductivities of acid-swollen S-P-S membranes. Fig. 3a and b shows Nyquist plots of S-P-S/Sa(80) and S-P-S/Pa(80) membranes with almost the same size by varying temperatures from $50\text{ }^{\circ}\text{C}$ to $95\text{ }^{\circ}\text{C}$, respectively. The vertical and horizontal axes in Fig. 3 are the imaginary part ($-Z''$) and the real part (Z') of the complex impedance (Z), respectively. The nonzero Z' intercept in the plot was taken as R of the test specimen.^{83,84} In the measurement frequency range, the data of S-P-S/Sa(80) and S-P-S/Pa(80) did not represent a semicircle type plot which is often observed in Nyquist plots for PEMs probably because of relatively fast proton transport. It is evident that S-P-S/Sa(80) in Fig. 3a gives a R value of $1.6 \times 10^2\ \Omega$, which is clearly much lower than that of S-P-S/Pa(80) ($5.9 \times 10^2\ \Omega$) at $95\text{ }^{\circ}\text{C}$. Using these R values, the anhydrous conductivities (σ_{DCS}) of S-P-S/Sa(80) and S-P-S/Pa(80) were estimated to be 1.4×10^{-1} and $6.1 \times 10^{-2}\ \text{S cm}^{-1}$ at $95\text{ }^{\circ}\text{C}$ from eqn (2), respectively. As the temperature decreased, the nonzero Z' intercept of both S-P-S/Sa(80) and S-P-S/Pa(80) became higher; in other words, the R value increased as the temperature decreased.

We further determined σ_{DCS} for S-P-S/Sa and S-P-S/Pa with different acid contents using the same procedure and plotted them against the reciprocal of the absolute temperature (T) in Fig. 4. Table S1 (ESI[†]) also summarizes the values of σ_{DC} . For the



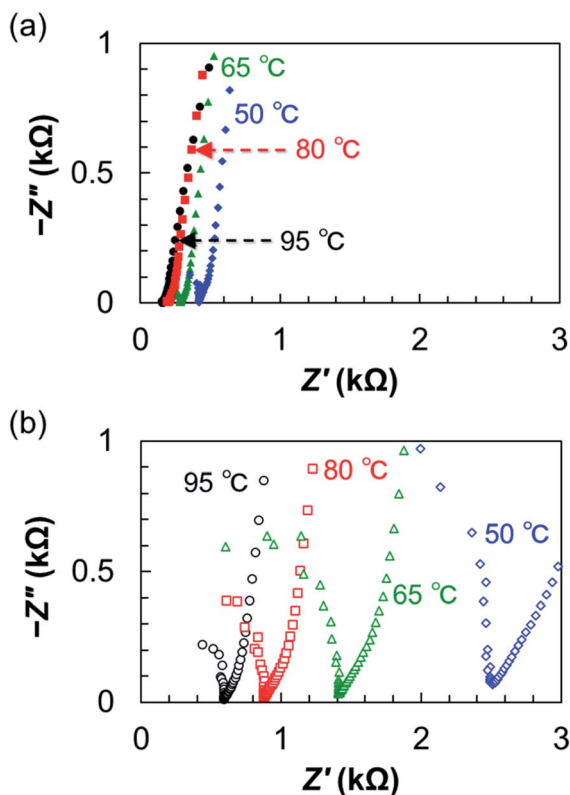


Fig. 3 Nyquist plots of membranes of (a) S-P-S/Sa(80) (filled symbols) and (b) S-P-S/Pa(80) (open symbols).

membranes with an Sa content below 40 wt%, the impedance spectra could not be correctly acquired due to a resistance higher than the detection limit. From Fig. 4, S-P-S/Sa(50) with an Sa content of 50 wt% exhibits the relatively low anhydrous σ_{DC} of $2.0 \times 10^{-4} \text{ S cm}^{-1}$ at 95 °C, while S-P-S/Sa(60) gives moderately high, $1.2 \times 10^{-2} \text{ S cm}^{-1}$ at the same temperature. It should be emphasized that the σ_{DC} suddenly increased by 2 orders of magnitude by adding merely 10 wt% more Sa. As the

Sa content increased further, S-P-S/Sa(70) and S-P-S/Sa(80) exhibit the higher σ_{DC} of around $10^{-1} \text{ S cm}^{-1}$; particularly, S-P-S/Sa(80) under anhydrous conditions records the very high conductivity of $1.4 \times 10^{-1} \text{ S cm}^{-1}$, which is comparable to that of humidified Nafion membranes, regardless of anhydrous conditions. Furthermore, even though ADL of S-P-S/Sa(80) was 4.6 that is lower than that of previously-reported high temperature-PEMs (HT-PEMs with ADL higher than 10), the anhydrous σ_{DC} of S-P-S/Sa(80) was higher than that of the HT-PEMs at around 100 °C. For example, a Pa-doped SPEEK/ionic liquid composite membrane with ADL of 10 exhibited the anhydrous σ_{DC} of $5.33 \times 10^{-2} \text{ S cm}^{-1}$ at 110 °C.⁵² Another example is a Pa-doped PBI/sulfonated titania composite membrane with ADL of 12.1, which showed the anhydrous σ_{DC} of $6.7 \times 10^{-2} \text{ S cm}^{-1}$ at 100 °C.⁵¹ These suggests that higher conductivities of S-P-S/Sa(80) should originate from the higher acidity of Sa than that of Pa. The results were also comparable to those from membranes of chemically cross-linked poly(4-vinylpyridine) swollen with Sa in our previous study; namely, the anhydrous conductivities of block polymer-based PEMs also strongly depended on the Sa content in the PEMs. It should be noted that σ_{DC} of S-P-S/Sa(80) at 95 °C was still around 94% of the initial σ_{DC} at 95 °C, even in approximately 330 hours after keeping the PEM at 95 °C (Fig. S5, ESI†). Furthermore, the S-P-S/Sa(80) membrane have retained the shape and high conductivities.

The σ_{DC} of membranes with a Pa content below 40 wt% was not correctly estimated, either, due to the very high resistance. On the other hand, S-P-S/Pa(50) exhibited the anhydrous σ_{DC} of $2.4 \times 10^{-4} \text{ S cm}^{-1}$, almost the same as that of S-P-S/Sa(50) at 95 °C. Below 80 °C, the σ_{DC} s of S-P-S/Pa(50) was lower than those of S-P-S/Sa(50). Similar to S-P-S/Sa membranes, the anhydrous σ_{DC} of S-P-S/Pa increased as the Pa content increased, and S-P-S/Pa(80) exhibited the comparatively high σ_{DC} of $6.1 \times 10^{-2} \text{ S cm}^{-1}$ at 95 °C. Roughly speaking, the σ_{DC} values for S-P-S/Pa membranes was lower than those for S-P-S/Sa with the same acid content.

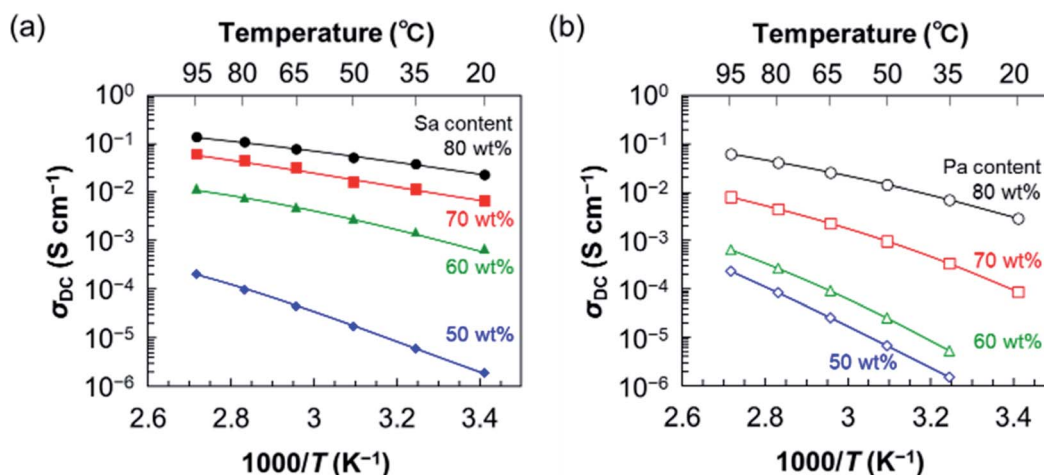


Fig. 4 Temperature dependence of anhydrous conductivity of a series of membranes of (a) S-P-S/Sa (filled symbols) and (b) S-P-S/Pa (open symbols). Solid lines are drawn just as guide for the eyes.



Fig. 4 also shows that the anhydrous σ_{DC} of S-P-S/Pa has a stronger temperature dependence than that of S-P-S/Sa at the same acid content. This is probably because highly acidic Sa would be almost completely dissociated into a hydrogen sulfate anion and a free proton in the membranes, even at low temperatures. Namely, the concentration of free protons in the S-P-S/Sa membrane would be almost constant regardless of temperatures; therefore, the main factor in the temperature dependence of anhydrous σ_{DC} could be the proton-hopping mechanism expressed by the Arrhenius equation with the activation energy.^{85,86} On the other hand, Pa with lower acidity would not be effectively dissociated into a dihydrogen phosphate anion and a free proton in the membranes at low temperatures near room temperature, whereas the dissociation of Pa becomes easier as the temperature increases. Therefore, the concentration of the free protons in S-P-S/Pa would increase as the temperature increases, resulting in the stronger temperature dependence of the anhydrous σ_{DC} for S-P-S/Pa, which is not followed by the Arrhenius equation.

3.3 Thermal analysis of acid-swollen S-P-S membranes

From the macroscopic appearance, it is apparent that both S-P-S/Sa and S-P-S/Pa membranes with acid content lower than 50 wt% were glassy and hard; in contrast, the samples with more than 60 wt% acid content were soft and gel-like

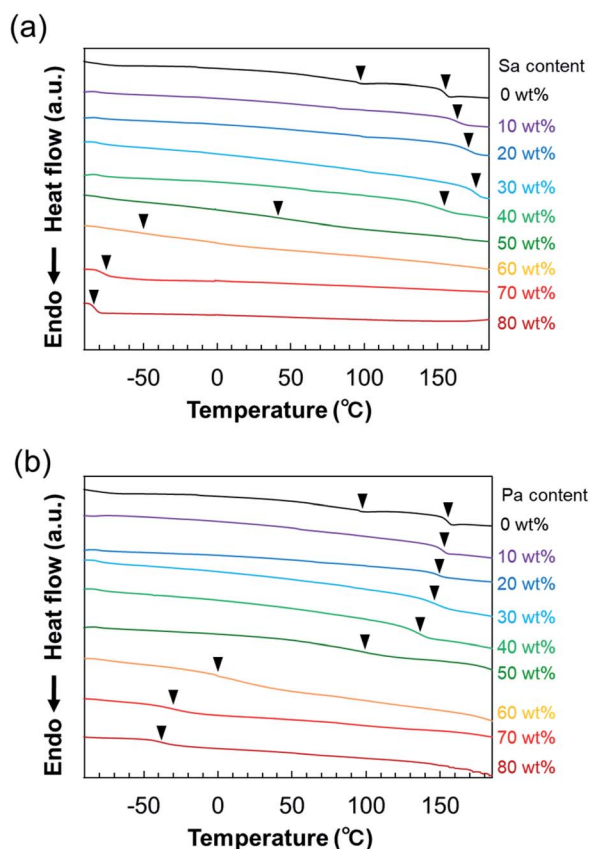


Fig. 5 DSC thermograms of a series of membranes of (a) S-P-S/Sa and (b) S-P-S/Pa.

membranes (see also Fig. S1, ESI[†]), indicating that the $T_{g,s}$ of the membranes were drastically affected by the acid content. DSC thermograms of the S-P-S/Sa and S-P-S/Pa membranes are shown in Fig. 5a and b, respectively, and the $T_{g,s}$ estimated from the thermograms are summarized in Table S2 (ESI[†]). The $T_{g,s}$ were observed at 96 °C and 155 °C in the thermogram of neat S-P-S without acid, which are due to the end S blocks and the middle P block, respectively. For both S-P-S/Sa and S-P-S/Pa membranes swollen with acid, the T_g originating from the S blocks cannot be read from the thermograms. This is because the volume fraction of S blocks in the acid-swollen membranes was actually much smaller than that of neat S-P-S upon addition of large amount of the acids. The T_g of the P-block-containing phase, *i.e.*, P/acid mixed phase in the S-P-S/Sa membranes slightly increased up to the Sa content of 30 wt%, and it decreased when the Sa content increased further; it should be noted that the T_g suddenly dropped at 50 wt% of Sa content. The T_g of the P/acid mixed phase in the S-P-S/Pa membranes also exhibited the same tendency as that for the S-P-S/Sa membranes.

The $T_{g,s}$ associated with the P block were plotted against the ADL and the acid weight content in the membranes in Fig. 6a to compare the acidity effects of two acids on the anhydrous σ_{DC} of the PEMs. At ADL < 1, where the stoichiometry of acid to the pyridyl group is below unity, the P/acid mixed phase in both S-P-S/Sa and S-P-S/Pa exhibited high $T_{g,s}$ above 140 °C. The results are presumably attributed to restricted segmental motions of polymer chains due to the formation of rigid acid-base complexes between the pyridyl groups and the acids in the membranes (see also the Fourier transform infrared spectra of S-P-S/Sa and S-P-S/Pa in Fig. S6 (ESI[†]), indicating the formation of the acid-base complex). The $T_{g,s}$ of the S-P-S/Sa membranes with ADL below unity were slightly higher than those of the S-P-S/Pa membranes, probably because the highly acidic Sa had a greater ability to form acid-base complexes. On the other hand, the $T_{g,s}$ of the P/acid mixed phase in both S-P-S/Sa and S-P-S/Pa underwent a sudden drop when ADL exceeded unity, since the excessive acid in the phase served as a plasticizer. It should also be noted that the $T_{g,s}$ of the S-P-S/Sa membranes were lower than those of the S-P-S/Pa membranes at ADL larger than unity, where Sa having a melting point (~ 10 °C)⁸⁷ lower than that of Pa (~ 42 °C)⁸⁸ can plasticize P polymer more effectively. Since the acids infiltrated into S-P-S/Sa or S-P-S/Pa served as both an agent for forming the acid-base complexes and a plasticizer to the P blocks, the variation in the $T_{g,s}$ of the P/acid mixed phase was not simple and did not agree with the Fox equation⁸⁹ (Fig. S7, ESI[†]) used to express the composition dependence on the T_g of blends composed of a polymer and a plasticizer.

The anhydrous σ_{DC} s of S-P-S/Sa and S-P-S/Pa at 95 °C were also plotted against ADL and the weight content of acid in Fig. 6b to compare the acidity effects of medium liquids on the σ_{DC} s of the PEMs. With ADL < 1, both S-P-S/Sa and S-P-S/Pa exhibited quite low σ_{DC} (close to 0 S cm⁻¹) at 95 °C. This is because there must be almost no free protons to contribute to the conductivity due to consumption of acids for forming the acid-base complexes between the pyridyl groups and the acids.



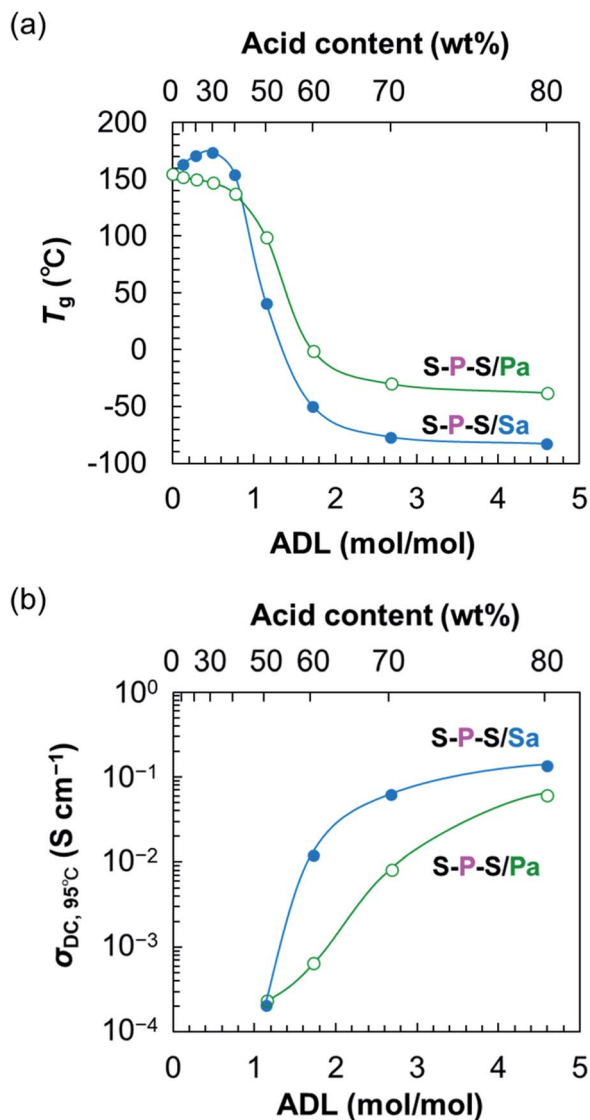


Fig. 6 (a) T_g of P/acid mixed phase and (b) anhydrous conductivity at 95 $^{\circ}\text{C}$ for a series of S-P-S/Sa and S-P-S/Pa membranes against ADL and the weight content of acid in the membranes. Solid lines are drawn as a guide for the eyes.

In addition, the restricted segmental motions of the polymer chains below the T_g s of the P/acid mixed phase probably lowered conductivity. On the other hand, when ADL exceeded unity, the segmental motions of the polymer chains became active owing to the sufficiently low T_g s of the P/acid mixed phase, and some free protons were released from an excessive amount of acid, resulting in enabling proton conduction in anhydrous conditions. As ADL increased further, these effects were enhanced and higher anhydrous σ_{DC} was attained.

Comparing S-P-S/Sa and S-P-S/Pa in Fig. 6b, S-P-S/Sa exhibited a higher anhydrous σ_{DC} than S-P-S/Pa when ADL was larger than unity. The tendency is probably due to two main reasons. First, the segmental motions of the P/acid mixed phase in S-P-S/Sa were more activated than those of S-P-S/Pa, which originates from the lower T_g s of the P/acid mixed complex

phase. Second, highly acidic Sa would be almost completely dissociated into a hydrogen sulfate anion and a free proton in the membranes, even at a low temperature. Note that Pa would not be effectively dissociated into a dihydrogen phosphate anion and a free proton in the membranes at low temperatures due to lower acidity.

4. Conclusions

A vinyl polymer-based S-P-S triblock copolymer was synthesized and swollen with Sa or Pa to investigate the effects of acidity of these two acidic liquids on anhydrous proton conductivity of the triblock copolymer-based PEMs. With ADL below unity, both S-P-S/Sa and S-P-S/Pa exhibited quite low conductivities under non-humidified conditions, because there were almost no free protons derived from the consumption of acids for forming the acid-base complexes between the pyridyl groups and the acids. On the other hand, when ADL exceeded unity, the T_g s of the P/acid mixed phase in both S-P-S/Sa and S-P-S/Pa suddenly dropped, and the PEMs exhibited moderate or high anhydrous conductivities. When ADL increased further, the concentration of free protons in the PEMs increased and the T_g s of the P/acid mixed phase decreased, revealing the high conductivities of both S-P-S/Sa and S-P-S/Pa under dry conditions, whereas S-P-S/Sa exhibited higher anhydrous conductivities than S-P-S/Pa. Notably, S-P-S/Sa(80) (ADL = 4.6) with a large amount of highly acidic Sa exhibited the very high conductivity of $1.4 \times 10^{-1} \text{ S cm}^{-1}$ at 95 $^{\circ}\text{C}$, even under dry conditions, which is comparable to that of humidified Nafion membranes and some non-humidified Pa-doped composite PEMs. It should be noted that anhydrous σ_{DC} had a stronger temperature dependency for S-P-S/Pa than for S-P-S/Sa with the same acid content, probably because highly acidic Sa would be almost completely dissociated into a hydrogen sulfate anion and a free proton in the PEMs, even at low temperatures near room temperature. On the other hand, Pa with a lower acidity would not be effectively dissociated into a dihydrogen phosphate anion and a free proton in the PEMs at low temperatures, but the dissociation of Pa would become easier as the temperature increased, resulting in an increase in the concentration of free protons in the S-P-S/Pa. The results in this study will help to design highly proton-conductive PEMs even under dry conditions at the molecular level for next-generation fuel cells. In the future, we will investigate the conductivities of such PEMs at temperatures lower than 20 $^{\circ}\text{C}$ or higher than 100 $^{\circ}\text{C}$ under non-humidified conditions. In addition, we will evaluate the mechanical properties of the PEMs, nanostructures, the cell performance, and the leaching-out of the acidic liquids in the PEMs, which will also provide useful insights on designing high performance anhydrous PEMs.

Author contributions

The manuscript was written with the contributions of all authors. All authors have given approval to the final version of the manuscript.



Conflicts of interest

There are no conflicts to declare.

Acknowledgements

The authors thank Mr Hikage at High Intensity X-ray Diffraction Laboratory in Nagoya University for his kind help in performing SAXS measurements. This work was partially supported through a project (JPN P20003) subsidized by the New Energy and Industrial Technology Development Organization (NEDO), and KAKENHI grant numbers (21K05197 (A. N.) and 20J11033 (T. K.)) from JSPS, Japan. A. N. is also grateful for Toyota Most Advanced Collaborative Research Grant.

References

- 1 B. C. H. Steele and A. Heinzl, *Nature*, 2001, **414**, 345–352.
- 2 A. Kirubakaran, S. Jain and R. K. Nema, *Renewable Sustainable Energy Rev.*, 2009, **13**, 2430–2440.
- 3 V. Das, S. Padmanaban, K. Venkitesamy, R. Selvamuthukumar, F. Blaabjerg and P. Siano, *Renewable Sustainable Energy Rev.*, 2017, **73**, 10–18.
- 4 M. A. Hickner, H. Ghassemi, Y. S. Kim, B. R. Einsla and J. E. McGrath, *Chem. Rev.*, 2004, **104**, 4587–4612.
- 5 S. J. Peighambaroust, S. Rowshanzamir and M. Amjadi, *Int. J. Hydrogen Energy*, 2010, **35**, 9349–9384.
- 6 H. Zhang and P. K. Shen, *Chem. Rev.*, 2012, **112**, 2780–2832.
- 7 A. Kraysberg and Y. Ein-Eli, *Energy Fuels*, 2014, **28**, 7303–7330.
- 8 Y. Wang, D. F. Ruiz Diaz, K. S. Chen, Z. Wang and X. C. Adroher, *Mater. Today*, 2020, **32**, 178–203.
- 9 T. E. Springer, T. A. Zawodzinski and S. Gottesfeld, *J. Electrochem. Soc.*, 1991, **138**, 2334–2342.
- 10 J. L. Lutkenhaus and P. T. Hammond, *Soft Matter*, 2007, **3**, 804–816.
- 11 S. Subianto, M. Pica, M. Casciola, P. Cojocar, L. Merlo, G. Hards and D. J. Jones, *J. Power Sources*, 2013, **233**, 216–230.
- 12 A. Kusoglu and A. Z. Weber, *Chem. Rev.*, 2017, **117**, 987–1104.
- 13 T. A. Zawodzinski, C. Derouin, S. Radzinski, R. J. Sherman, V. T. Smith, T. E. Springer and S. Gottesfeld, *J. Electrochem. Soc.*, 1993, **140**, 1041–1047.
- 14 Y. Sone, P. Ekdunge and D. Simonsson, *J. Electrochem. Soc.*, 1996, **143**, 1254–1259.
- 15 J. Peron, A. Mani, X. Zhao, D. Edwards, M. Adachi, T. Soboleva, Z. Shi, Z. Xie, T. Navessin and S. Holdcroft, *J. Membr. Sci.*, 2010, **356**, 44–51.
- 16 T. D. Gierke, G. E. Munn and F. C. Wilson, *J. Polym. Sci., Polym. Phys. Ed.*, 1981, **19**, 1687–1704.
- 17 K. A. Mauritz and R. B. Moore, *Chem. Rev.*, 2004, **104**, 4535–4586.
- 18 K. Schmidt-Rohr and Q. Chen, *Nat. Mater.*, 2008, **7**, 75–83.
- 19 M. Rikukawa and K. Sanui, *Prog. Polym. Sci.*, 2000, **25**, 1463–1502.
- 20 D. W. Shin, M. D. Guiver and Y. M. Lee, *Chem. Rev.*, 2017, **117**, 4759–4805.
- 21 P. Xing, G. P. Robertson, M. D. Guiver, S. D. Mikhailenko, K. Wang and S. Kaliaguine, *J. Membr. Sci.*, 2004, **229**, 95–106.
- 22 A. Iulianelli and A. Basile, *Int. J. Hydrogen Energy*, 2012, **37**, 15241–15255.
- 23 M. J. Parnian, S. Rowshanzamir and F. Gashoul, *Energy*, 2017, **125**, 614–628.
- 24 F. Lufano, I. Gatto, P. Staiti, V. Antonucci and E. Passalacqua, *Solid State Ionics*, 2001, **145**, 47–51.
- 25 L. Li and Y. Wang, *J. Power Sources*, 2006, **162**, 541–546.
- 26 B. Lafitte and P. Jannasch, *Adv. Funct. Mater.*, 2007, **17**, 2823–2834.
- 27 Y. Chang, A. D. Mohanty, S. B. Smedley, K. Abu-Hakme, Y. H. Lee, J. E. Morgan, M. A. Hickner, S. S. Jang, C. Y. Ryu and C. Bae, *Macromolecules*, 2015, **48**, 7117–7126.
- 28 L. Wang, N. Deng, G. Wang, J. Ju, B. Cheng and W. Kang, *ACS Appl. Mater. Interfaces*, 2019, **11**, 39979–39990.
- 29 M. A. Hickner, C. H. Fujimoto and C. J. Cornelius, *Polymer*, 2006, **47**, 4238–4244.
- 30 J. Miyake, R. Taki, T. Mochizuki, R. Shimizu, R. Akiyama, M. Uchida and K. Miyatake, *Sci. Adv.*, 2017, **3**, ea00476.
- 31 E. G. Sorte, B. A. Paren, C. G. Rodriguez, C. Fujimoto, C. Poirier, L. J. Abbott, N. A. Lynd, K. I. Winey, A. L. Frischknecht and T. M. Alam, *Macromolecules*, 2019, **52**, 857–876.
- 32 J. Kim, B. Kim and B. Jung, *J. Membr. Sci.*, 2002, **207**, 129–137.
- 33 M. J. Park, K. H. Downing, A. Jackson, E. D. Gomez, A. M. Minor, D. Cookson, A. Z. Weber and N. P. Balsara, *Nano Lett.*, 2007, **7**, 3547–3552.
- 34 R. Bouchet and E. Siebert, *Solid State Ionics*, 1999, **118**, 287–299.
- 35 M. Yamada and I. Honma, *Polymer*, 2005, **46**, 2986–2992.
- 36 S. R. Narayanan, S.-P. Yen, L. Liu and S. G. Greenbaum, *J. Phys. Chem. B*, 2006, **110**, 3942–3948.
- 37 Q. Li, J. O. Jensen, R. F. Savinell and N. J. Bjerrum, *Prog. Polym. Sci.*, 2009, **34**, 449–477.
- 38 S. Bureekaew, S. Horike, M. Higuchi, M. Mizuno, T. Kawamura, D. Tanaka, N. Yanai and S. Kitagawa, *Nat. Mater.*, 2009, **8**, 831–836.
- 39 S.-Y. Lee, A. Ogawa, M. Kanno, H. Nakamoto, T. Yasuda and M. Watanabe, *J. Am. Chem. Soc.*, 2010, **132**, 9764–9773.
- 40 R. Sood, A. Donnadio, S. Giancola, A. Kreisz, D. J. Jones and S. Cavaliere, *ACS Appl. Mater. Interfaces*, 2016, **8**, 16897–16906.
- 41 K.-S. Lee, J. S. Spindel, Y.-K. Choe, C. Fujimoto and Y. S. Kim, *Nat. Energy*, 2016, **1**, 16120.
- 42 X. Li, H. Ma, P. Wang, Z. Liu, J. Peng, W. Hu, Z. Jiang, B. Liu and M. D. Guiver, *Chem. Mater.*, 2020, **32**, 1182–1191.
- 43 V. Atanasov, A. S. Lee, E. J. Park, S. Maurya, E. D. Baca, C. Fujimoto, M. Hibbs, I. Matanovic, J. Kerres and Y. S. Kim, *Nat. Mater.*, 2021, **20**, 370–377.
- 44 J. S. Wainright, J. T. Wang, D. Weng, R. F. Savinell and M. Litt, *J. Electrochem. Soc.*, 1995, **142**, L121–L123.
- 45 M. Linlin, A. K. Mishra, N. H. Kim and J. H. Lee, *J. Membr. Sci.*, 2012, **411–412**, 91–98.
- 46 E. Quartarone, P. Mustarelli, A. Carollo, S. Grandi, A. Magistris and C. Gerbaldi, *Fuel Cells*, 2009, **9**, 231–236.



- 47 R. Kannan, H. N. Kagalwala, H. D. Chaudhari, U. K. Kharul, S. Kurungot and V. K. Pillai, *J. Mater. Chem.*, 2011, **21**, 7223–7231.
- 48 Suryani, C.-M. Chang, Y.-L. Liu and Y. M. Lee, *J. Mater. Chem.*, 2011, **21**, 7480–7486.
- 49 Suryani, Y.-N. Chang, J.-Y. Lai and Y.-L. Liu, *J. Membr. Sci.*, 2012, **403–404**, 1–7.
- 50 F. J. Pinar, P. Cañizares, M. A. Rodrigo, D. Ubeda and J. Lobato, *RSC Adv.*, 2012, **2**, 1547–1556.
- 51 S. Lee, K. Seo, R. V. Ghorpade, K.-H. Nam and H. Han, *Mater. Lett.*, 2020, **263**, 127167.
- 52 Q. Che, R. He, J. Yang, L. Feng and R. F. Savinell, *Electrochem. Commun.*, 2010, **12**, 647–649.
- 53 R. Kumar, M. Mamlouk and K. Scott, *RSC Adv.*, 2014, **4**, 617–623.
- 54 Q. Che, L. Zhou and J. Wang, *J. Mol. Liq.*, 2015, **206**, 10–18.
- 55 S. Singha and T. Jana, *ACS Appl. Mater. Interfaces*, 2014, **6**, 21286–21296.
- 56 S. R. Kutcherlapati, R. Koyilapu and T. Jana, *J. Polym. Sci., Part A: Polym. Chem.*, 2018, **56**, 365–375.
- 57 S. Mukhopadhyay, A. Das, T. Jana and S. K. Das, *ACS Appl. Energy Mater.*, 2020, **3**, 7964–7977.
- 58 C. M. Bates and F. S. Bates, *Macromolecules*, 2017, **50**, 3–22.
- 59 N. Hampu, J. R. Werber, W. Y. Chan, E. C. Feinberg and M. A. Hillmyer, *ACS Nano*, 2020, **14**, 16446–16471.
- 60 Y. He, P. G. Boswell, P. Bühlmann and T. P. Lodge, *J. Phys. Chem. B*, 2007, **111**, 4645–4652.
- 61 T. P. Lodge, *Science*, 2008, **321**, 50–51.
- 62 A. Noro, M. Hayashi and Y. Matsushita, *Soft Matter*, 2012, **8**, 6416.
- 63 M. Watanabe, M. L. Thomas, S. Zhang, K. Ueno, T. Yasuda and K. Dokko, *Chem. Rev.*, 2017, **117**, 7190–7239.
- 64 S. Y. Kim, S. Kim and M. J. Park, *Nat. Commun.*, 2010, **1**, 88.
- 65 M. L. Hoarfrost and R. A. Segalman, *Macromolecules*, 2011, **44**, 5281–5288.
- 66 S. A. Chopade, S. So, M. A. Hillmyer and T. P. Lodge, *ACS Appl. Mater. Interfaces*, 2016, **8**, 6200–6210.
- 67 T. Kajita, H. Tanaka, A. Noro, Y. Matsushita and N. Nakamura, *J. Mater. Chem. A*, 2019, **7**, 15585–15592.
- 68 J. Chiefari, Y. K. Chong, F. Ercole, J. Krstina, J. Jeffery, T. P. T. Le, R. T. A. Mayadunne, G. F. Meijs, C. L. Moad, G. Moad, E. Rizzardo and S. H. Thang, *Macromolecules*, 1998, **31**, 5559–5562.
- 69 G. Moad, E. Rizzardo and S. H. Thang, *Aust. J. Chem.*, 2005, **58**, 379.
- 70 J. T. Lai, D. Filla and R. Shea, *Macromolecules*, 2002, **35**, 6754–6756.
- 71 K. H. Noro, Y. Sageshima and Y. Matsushita, *Macromolecules*, 2012, **45**, 8013–8020.
- 72 K. Nieswandt, P. Georgopoulos, C. Abetz, V. Filiz and V. Abetz, *Materials*, 2019, **12**, 3145.
- 73 K. Nieswandt, P. Georgopoulos and V. Abetz, *Polym. Chem.*, 2021, **12**, 2210–2221.
- 74 Y. Kang, J. J. Walsh, T. Gorishnyy and E. L. Thomas, *Nat. Mater.*, 2007, **6**, 957–960.
- 75 A. Noro, Y. Tomita, Y. Shinohara, Y. Sageshima, J. J. Walsh, Y. Matsushita and E. L. Thomas, *Macromolecules*, 2014, **47**, 4103–4109.
- 76 A. Noro, Y. Tomita, Y. Matsushita and E. L. Thomas, *Macromolecules*, 2016, **49**, 8971–8979.
- 77 M. F. Schulz, A. K. Khandpur, F. S. Bates, K. Almdal, K. Mortensen, D. A. Hajduk and S. M. Gruner, *Macromolecules*, 1996, **29**, 2857–2867.
- 78 Y. Matsushita, K. Mori, R. Saguchi, Y. Nakao, I. Noda and M. Nagasawa, *Macromolecules*, 1990, **23**, 4313–4316.
- 79 A. Noro, D. Cho, A. Takano and Y. Matsushita, *Macromolecules*, 2005, **38**, 4371–4376.
- 80 C. H. Lee, H. B. Park, Y. M. Lee and R. D. Lee, *Ind. Eng. Chem. Res.*, 2005, **44**, 7617–7626.
- 81 S.-E. Nam, S.-O. Kim, Y. Kang, J. W. Lee and K.-H. Lee, *J. Membr. Sci.*, 2008, **322**, 466–474.
- 82 O. Altintas, K. Riazi, R. Lee, C. Y. Lin, M. L. Coote, M. Wilhelm and C. Barner-Kowollik, *Macromolecules*, 2013, **46**, 8079–8091.
- 83 R. L. Weber, Y. Ye, S. M. Banik, Y. A. Elabd, M. A. Hickner and M. K. Mahanthappa, *J. Polym. Sci. Part B Polym. Phys.*, 2011, **49**, 1287–1296.
- 84 M. L. Hoarfrost and R. A. Segalman, *ACS Macro Lett.*, 2012, **1**, 937–943.
- 85 C. J. T. Grotthuss, *Ann. Chim.*, 1806, **LVIII**, 54–74.
- 86 N. Agmon, *Chem. Phys. Lett.*, 1995, **244**, 456–462.
- 87 T. Ohtake, *Tellus B Chem. Phys. Meteorol.*, 1993, **45**, 138–144.
- 88 T. Dippel, K. D. Kreuer, J. C. Lassegues and D. Rodriguez, *Solid State Ionics*, 1993, **61**, 41–46.
- 89 M. A. B. H. Susan, T. Kaneko, A. Noda and M. Watanabe, *J. Am. Chem. Soc.*, 2005, **127**, 4976–4983.

